Formamidinium incorporation into compact lead iodide for low bandgap perovskite solar cells with open-circuit voltage approaching the radiative limit

Hui Zhang,[†,‡] Mariia Kramarenko,[†] Guillermo Martínez-Denegri,[†] Johann Osmond,[†] Johann Toudert,*[†] and Jordi Martorell*[†,⊥]*

[†]ICFO – Institut de Ciències Fotòniques, The Barcelona Institute of Science and Technology, 08860 Castelldefels (Barcelona), Spain

[‡]Key Laboratory of Flexible Electronics (KLOFE) and Institute of Advanced Materials (IAM), Jiangsu National Synergetic Innovation Center for Advanced Materials (SICAM), Nanjing Tech University (NanjingTech), Nanjing, P.R. China

[⊥]Departament de Física, Universitat Politècnica de Catalunya, 08222 Terrassa, Spain

KEYWORDS: solar cells, perovskite, open-circuit voltage, fluorescence quantum yield, radiative limit

ABSTRACT: To bring hybrid lead halide perovskite solar cells towards the Shockley-Queisser limit requires lowering the bandgap while simultaneously increasing the open circuit voltage. This, to some extent divergent objective, may demand the use of large cations to obtain a perovskite with larger lattice parameter together with a large crystal size to minimize interface non-radiative recombination. When applying the two-step method for a better crystal control, it is rather challenging to fabricate perovskites with FA^+ cations, given the small penetration depth of such large ions into a compact PbI_2 film. In here, to successfully incorporate such large cations, we used a high concentration solution of the organic precursor containing small Cl^- anions achieving, via a solvent annealing-controlled dissolution-recrystallization, larger than 1 μm perovskite crystals in a solar cell. This solar cell, with a largely increased fluorescence quantum yield, exhibited an open circuit voltage equivalent to 93% of the corresponding radiative limit one. This, together with the low bandgap achieved (1.53 eV), makes the fabricated perovskite cell one of the closest to the Shockley-Queisser optimum.

1. INTRODUCTION

Hybrid lead halide perovskites have become one of the most promising semiconductors in the last decade owing to their excellent optoelectronic properties, simple solution processed fabrication and broad application potential. In a short period of time perovskite based solar cells have reached a remarkably good performance[1-5] with certified power conversion efficiencies up to 23.7%.[1] Although this figure is certainly impressive, it still lies more than one percentage point below the efficiency from large area silicon laboratory cells[6] and more than ten percentage points below the Shockley–Queisser efficiency limit for planar geometry single junction solar cells.[5,7]

An important step towards that latter limit requires lowering the band gap of the active perovskite layer to 1.35 eV, i.e. by about 0.2 eV with respect to that of the standard methylammonium lead iodide perovskite ($MAPbI_3$, 1.57 eV). By increasing the size of the A^+ cation in the perovskite ABX_3 lattice, one may achieve an expansion of the lattice parameter, which in most of the cases turns into a red shift in the absorption or a lower band gap approaching the optimal 1.35 eV value. The smallest bandgap achieved for a hybrid lead halide perovskite, 1.48 eV, has been reported when formamidinium (FA^+) is used as the A^+ cation.[8,9] However, the active (black) trigonal phase of $FAPbI_3$ that presents such band gap is unstable in ambient conditions, where it undergoes a transition to an inactive (yellow) wide band gap hexagonal phase.[10] Improved stability has been demonstrated with mixed cation/anion hybrid lead halide perovskites that incorporate several cations and/or anions among FA^+, MA^+, Rb^+, Cs^+, Br^-, I^-, Cl^-.[1-4, 11-16] Especially, introducing MA^+ cations into $FAPbI_3$ enables stabilizing the active trigonal phase while maintaining a smaller band gap than $MAPbI_3$.[10,16]

Simultaneously with achieving a band gap as close as possible to 1.35 eV, V_{oc} should be increased towards its ideal value (or radiative limit), reached when photon emission from direct conduction-to-valence band transitions in the perovskite layer is the sole charge recombination mechanism in the cell at open circuit. It is realistic to assume that the optimal V_{oc} required for

reaching Shockley–Queisser limit efficiencies is achievable in perovskite cells provided that close to 100% external fluorescence quantum yields have been measured in single crystals of $MAPbI_3$.[17] Towards such optimal V_{oc} in perovskite solar cells, non-radiative contributions to charge recombination in the perovskite layer must be minimized. In such layer, typically with a polycrystalline structure, non-radiative recombination may occur especially on defects at crystal interfaces. Passivation of these interface defects has been shown very recently to boost the external fluorescence quantum yield of mixed cation/anion perovskites.[18] An alternative to such passivation process consists in growing large, high-quality crystals to maximize the probability of bulk radiative recombination with respect to non-radiative recombination at crystal interfaces. Indeed, it has been shown that an increase in the size of the crystals in the perovskite layer decreases the probability of interface recombination, and recombination rate values approaching the lower bulk rates can be achieved when crystals larger than 30 μm are grown.[19]

In planar solar cells, a perovskite layer with large, high-quality crystals *and* a tuned band gap may be grown following the "two-step" fabrication method, which provides a path for controlling *separately* the crystal size and composition.[20,21] This method contrasts with the "one-step" method, which may offer less flexibility when a decoupled control of the crystal size *and* composition is targeted, provided it involves *simultaneously* chemical transformation, mass transport, nucleation and crystal growth.[10-15] Note, however, that recent progresses in solvent engineering have opened the way to an improved flexibility of the one-step method, suitable for a practical fabrication of high-efficiency and high-stability devices.[18]

In the first step of the two-step method, a crystalline PbI_2 film is grown by spin-coating. In the second step, an organic precursor solution is spun onto this film. After inter-diffusion of this precursor into PbI_2, perovskite crystals nucleate and grow to form the final layer. Because the PbI_2 film acts as a template for the nucleation-growth of the perovskite, controlling its nano-structure is one of the keys toward an efficient tuning of the perovskite crystal size. Strategies

for such a nanostructure control have already been reported, showing the way to achieve compact or porous PbI_2 films.[22,23] Another key to grow a perovskite with large crystals is enabling an efficient inter-diffusion of the organic precursor into the PbI_2 crystal lattice. This is a particularly critical aspect, because of the typically short penetration depth of the organic precursor into this lattice, which may lead to an incomplete PbI_2-to-perovskite chemical conversion that can be detrimental for the solar cell performance.

In contrast with the one-step method that has been applied for a broad exploration of the perovskite compositional space,[12,18] the two-step method has been used mainly for the fabrication of $MAPbI_3$ perovskites.[21] One of the strategies found for maximizing the PbI_2-to-$MAPbI_3$ conversion efficiency consisted in using a porous PbI_2 film as template.[24,25] The organic precursor solution infiltrates into the pores, where it reacts at the surface of the PbI_2 crystals. Even if the penetration depth of the organic precursor into these crystals remains small, their high surface-to-volume ratio in the porous film enables an efficient PbI_2-to-$MAPbI_3$ conversion. Using porous PbI_2 films as template has also allowed to fabricate mixed cation/anion hybrid lead halide perovskites, although with a much smaller number of reports than for the $MAPbI_3$ ones.[26-32] Specially, porosity enables the efficient incorporation of the larger FA^+ cations into the PbI_2 lattice.[32] Unfortunately, porosity generally also sets an upper limit to the final size of the perovskite crystals, which is affected by the dimensions and density of the initial PbI_2 structures. Although realizing a multi-step deposition of the organic precursor on porous PbI_2 has been shown to relax this limitation,[33] using compact PbI_2 films as template for MA^+ cation incorporation instead of the porous one appeared as an ideal way to overcome the upper limit imposed on the crystal size in $MAPbI_3$ perovskites in a genuinely two-step process.[34] To achieve a complete conversion of the compact PbI_2 into $MAPbI_3$, using a highly concentrated organic precursor solution was necessary. Indeed, for a too low concentration (typically, less than 10 mg/mL), the conversion occurs only partially, and is localized at the surface of the PbI_2 material where the formed perovskite acts as a barrier that prohibits the

conversion of the PbI_2 underneath.[35] For a high enough concentration (typically, of a few tens of mg/mL), such solution temporarily dissolves the PbI_2 lattice as well as any already formed surface perovskite layer. This facilitates the in-depth intercalation of the MA^+ cations, which is followed by the nucleation and growth of perovskite crystals. Such "dissolution-crystallization" mechanism enables a deep PbI_2-to-$MAPbI_3$ conversion even if the PbI_2 template is compact. Note that the concentration needed to achieve such deep conversion may depend on the experimental conditions, such as temperature or PbI_2 thickness. In contrast, it is particularly challenging to fabricate hybrid lead halide perovskites based on larger cations such as FA^+ using a compact PbI_2 film as template, where the penetration depth of such ions is smaller than that of the MA^+ ones. In that case using a highly concentrated organic precursor is not sufficient by itself, and as was recently pointed out in a review by H. Chen,[21] the compositions of the template and/or organic precursor solution need to be well controlled to achieve an optimal crystal quality for the final perovskite layer.

In here, to grow a mixed cation (FA^+, MA^+) hybrid lead iodide perovskite with large high-quality crystals using the two-step method, we used a compact PbI_2 film as template. To tackle the challenge of promoting a complete conversion of compact PbI_2 into large high-quality perovskite crystals incorporating the large FA^+ cations, we considered adding small Cl^- anions into the highly concentrated organic precursor solution (> 60 mg/mL) together with realizing a solvent annealing after the spin-coating of this solution. Cl^- anions have been shown to ease the dissolution of PbI_2 crystals required for an efficient cation incorporation[36] and boost the optoelectronic quality of the final perovskite,[37, 38] and the realization of a post spin-coating solvent annealing facilitates mass transport and the growth of perovskite crystals.[39,40] We show that, only when all these synthesis conditions are fulfilled together, a high-quality mixed cation (FA^+, MA^+) hybrid lead iodide perovskite is formed. Following such approach, we obtained high-quality $FA_{0.8}MA_{0.2}PbI_3$ crystals larger than 1 μm in the lateral dimension of a perovskite layer close to 400 nm - thick. The crystals in this layer presented a smaller bandgap than the

$MAPbI_3$ perovskite owing to the successful FA^+ cation incorporation and did not contain any trace of the inactive wide bandgap hexagonal phase. The measured external fluorescence quantum yield of such layer grown on top of TiO_2 was near 5 times larger than the one from a layer with the same thickness grown also on top of TiO_2 but following a standard two-step procedure using a porous PbI_2 film as template. Measurements of the photovoltaic performance on series of cells indicated that the most probable V_{oc} value is 70 mV larger when the perovskite layer is grown using a compact PbI_2 film than when it is grown using a porous one. It is estimated that the highest V_{oc} achieved in this work lags only 80 mV below the ideal, radiative limit value, or in other words, it reaches 93% of the ideal value. Note that such V_{oc} is achieved for a perovskite bandgap as low as 1.53 eV, making the proposed fabrication approach suitable for tackling the challenge of simultaneously bringing V_{oc} and bandgap close to their optimal Schockley-Queisser values.

2. RESULTS

2.1. Compact PbI_2 – templated growth for the fabrication of high-quality micro-crystal $FA_{1-x}MA_xPbI_3$ perovskites

To fabricate a high crystal quality $FA_{1-x}MA_xPbI_3$ perovskite by the two-step method, we developed an approach (called hereafter "compact PbI_2 – templated perovskite growth") whose main steps are depicted in Figure 1a.

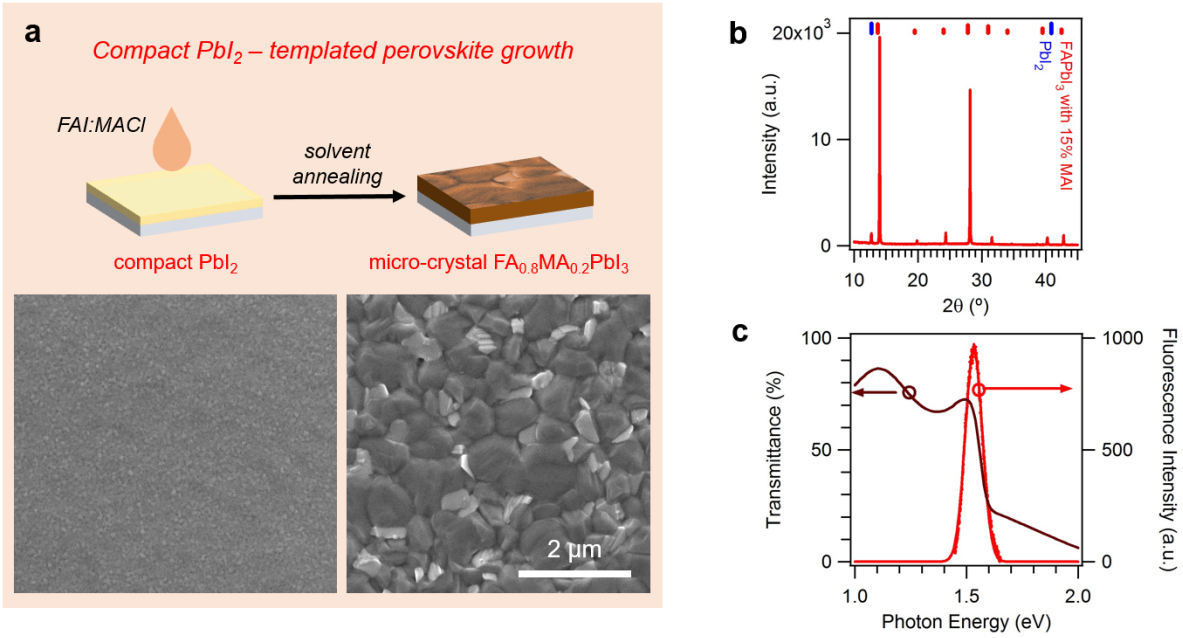

Figure 1. Two-step deposition: compact PbI_2 – templated perovskite growth to achieve a high-quality micro-crystal $FA_{0.8}MA_{0.2}PbI_3$ perovskite layer. (a) This approach consists in spin-coating a FAI:MACl solution onto a compact PbI_2 film, followed by a solvent annealing (top panel). Because the initial PbI_2 layer can be considered as a single structure (bottom left panel, top-view SEM image), it does not limit the lateral growth of the perovskite crystals whose lateral size reaches beyond 1 µm (bottom right panel, top-view SEM image). (b) XRD pattern of the fabricated perovskite layer. The position of the main diffraction peaks of PbI_2 and a mixed cation hybrid lead halide perovskite ($FAPbI_3$ with 15% MAI, from ref. 10) are shown at the top for comparison. (c) Transmittance and fluorescence spectra of the fabricated perovskite layer.

Schematic diagrams of this approach are provided in Supporting Information S1. A high-concentration FAI:MACl organic solution is spun onto a compact PbI_2 film, followed by a solvent annealing that consists in annealing the material under a solvent vapour.[39,40] By combining the effects of the highly concentrated organic precursor solution, Cl^- addition, and solvent annealing, this approach enables an efficient inter-diffusion of the organic precursor into the compact PbI_2 lattice, and the formation of a perovskite layer with crystal lateral dimensions larger than 1 µm as seen in the SEM image from Figure 1a.

As shown by the XRD pattern of the fabricated perovskite layer plotted in Figure 1b, the compact PbI_2 – templated growth approach enables the formation of perovskite crystals without any trace of the hexagonal phase. The peak positions, weakly shifted toward large angles compared with a reference $FA_{0.85}MA_{0.15}PbI_3$ pattern,[10] indicate slightly smaller lattice dimensions i.e. a slightly higher MA^+ content. This is consistent with the expected composition,

$FA_{0.8}MA_{0.2}PbI_3$. Note that the proposed final composition does not include chlorine, which even if introduced during the preparation, is usually not present with a significant concentration in hybrid lead halide perovskites, owing to the small radius of the Cl^- anion that makes it easy to exodiffuse from the crystal lattice.[26] The XRD pattern also indicates that a small amount of PbI_2 is present, probably indicating a surface self-passivation of the perovskite crystals rather than the presence of unreacted PbI_2. This will be confirmed from cross-section SEM images in section 2.3.

The transmittance and fluorescence spectra of the fabricated perovskite layer represented in Figure 1c show, respectively, the perovskite absorption onset and the radiative recombination peak both near 1.52 – 1.53 eV (810 nm). Such values confirm that the bandgap of the fabricated perovskite layer is narrower than that of $MAPbI_3$ perovskites (1.57 eV), as targeted by the FA^+ incorporation.

Note that, for the growth of crystals with the targeted large size and excellent optoelectronic properties using the compact PbI_2 – templated growth, a deliberate choice of specific and suitable fabrication conditions, combining the Cl^- anion addition to a highly-concentrated organic precursor with a post-spin coating solvent annealing, is mandatory. As can be seen again in Figure 2**,** in such conditions (FAI:MACl + solvent annealing) one can obtain perovskite crystals with sizes above 1 μm. These are significantly larger than the crystal sizes one may achieve when following other more simple procedures where no Cl^- anions are added to the organic precursor (FAI:MAI + solvent annealing), or a standard thermal annealing is performed instead of the solvent annealing (FAI:MACl + thermal annealing), or a standard thermal annealing is performed with no Cl^- anions (FAI:MAI + thermal annealing). Without Cl^- anion addition, the dissolution of the compact PbI_2 template required for FA^+ ion incorporation is not efficient thus leading to a limited perovskite crystal nucleation. During a standard thermal annealing, which is performed without solvent vapor, a poor mass transport takes place thus limiting the growth of the perovskite crystals.

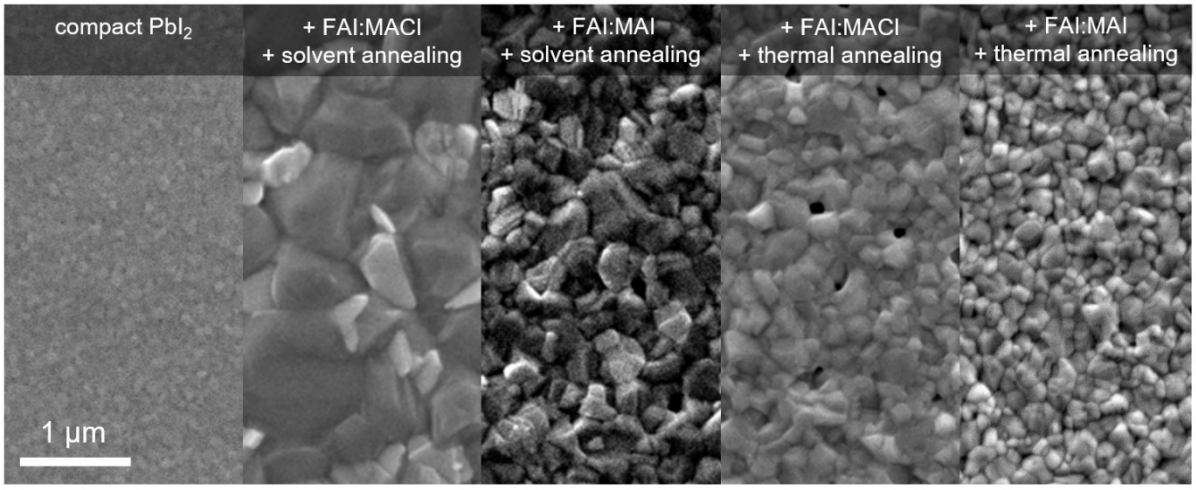

Figure 2. Necessary combination of Cl^- incorporation to a highly-concentrated organic precursor and post-spin coating solvent annealing to grow a micro-crystal $FA_{0.8}MA_{0.2}PbI_3$ perovskite layer with the compact PbI_2 – templated growth approach. This figure shows the top-view SEM images of the initial compact PbI_2 film, and of perovskite films formed from it after: FAI:MACl + solvent annealing; FAI:MAI spin-coating + solvent annealing (no Cl^-); FAI:MACl + thermal annealing (no solvent annealing); FAI:MAI + thermal annealing (no Cl^-, no solvent annealing). A micro-crystal perovskite is obtained only with the combination of Cl^- incorporation and solvent annealing.

To establish a reference for the study of the fluorescence and photovoltaic properties of the compact PbI_2 – templated perovskites, we also grew $FA_{0.8}MA_{0.2}PbI_3$ perovskite layers following the "standard" approach based on using a porous PbI_2 film as template. Schematic diagrams of this approach are provided in Supporting Information S1. With this approach that is called hereafter "porous PbI_2 – templated growth", the perovskite formed consists of smaller crystals than the compact PbI_2 – templated one, while presenting a similar position for its optical absorption onset and radiative recombination peak. This is further discussed in Supporting Information S2 and S3.

2.2. Impact of the perovskite crystal size on the fluorescence quantum yield

To evaluate the contribution of radiative and non-radiative recombination paths for photocarriers in the compact PbI_2 – templated and porous PbI_2 – templated perovskite layers, the external fluorescence quantum yield of such layers grown on a TiO_2 layer was measured using an integrated sphere – based setup depicted in Figure 3a.

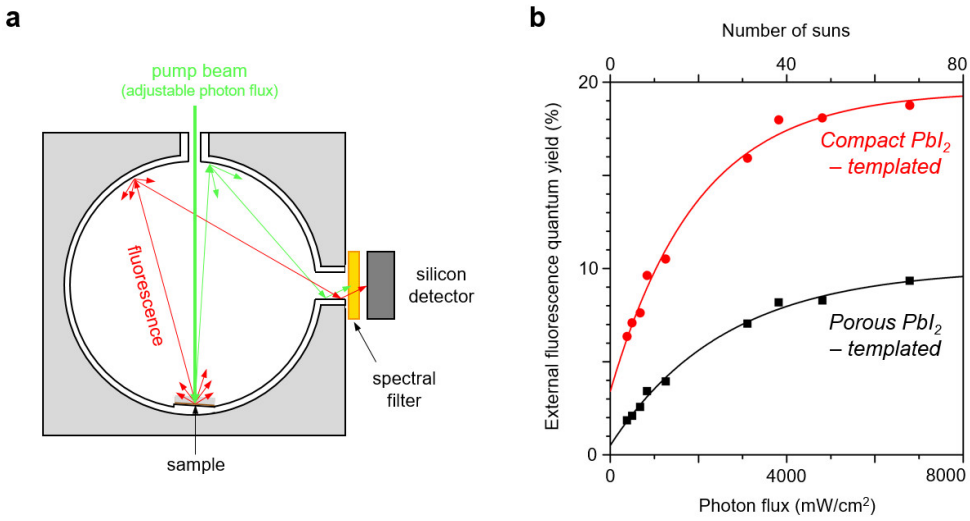

Figure 3. External fluorescence quantum yield of perovskite layers fabricated by compact PbI_2 – templated and porous – PbI_2 templated growth approaches. (a) Schematic representation of the external fluorescence quantum yield measurement setup. A green pump laser beam (wavelength of 532 nm) is shined onto the sample placed inside an integrating sphere. The sample consists of a perovskite/TiO_2 bilayer grown a glass substrate and light impinges onto the perovskite through the glass and TiO_2. The pump light unabsorbed by the perovskite and the light emitted by it (wavelength near 810 nm) are detected selectively with a calibrated silicon detector by introducing adequate spectral filters. The external fluorescence quantum yield was measured for different incident photon fluxes, increasing up to the equivalent of 70 suns. Further details are given in the Experimental section. (b) Measured external fluorescence quantum yield as a function of the incident photon flux. The compact PbI_2 – templated perovskite layer shows a higher external fluorescence quantum yield at all fluxes than the porous PbI_2 – templated one. The flux dependence of the external fluorescence quantum yield (increase-saturation) indicates the predominance of a trap-filling mechanism for both kinds of perovskites.

As shown in Figure 3b, the perovskite layers fabricated by the two approaches present a high external fluorescence quantum yield, with a photon flux – dependent (increase-saturation) behavior that indicates that a trap-filling mechanism takes place.[41,42] The different perovskite crystal size achieved with the two approaches has a strong controllable impact on the external fluorescence quantum yield. The compact PbI_2 – templated perovskite layer, which has the largest crystals, presents the highest external fluorescence quantum yield at all photon fluxes, with values near 4% for a 1 sun – equivalent illumination, and near 20% at saturation, for a 70 sun – equivalent illumination. These are among the highest values found in the literature without specific passivation treatment,[1,42-44] suggesting a particularly high contribution of radiative recombination paths, i.e. a particularly low defect density. Note that the external fluorescence quantum yield of the porous PbI_2 – templated perovskite layer for a 70 sun –

equivalent illumination reaches only 8%, suggesting the existence of another type of (non-saturable) defects opening additional non-radiative recombination paths.

2.3. Impact of the perovskite crystal size on solar cell performance

The crystal size in the fabricated perovskite layers impacts the photovoltaic properties of solar cells based on them. Whereas series of 50 cells were fabricated following each approach, we first focused on comparing the nanostructure and photovoltaic properties of selected cells of each type, as examples representative of the trends over the whole series. Cross-section SEM images corresponding to cells of the two types are shown in Figure 4a.

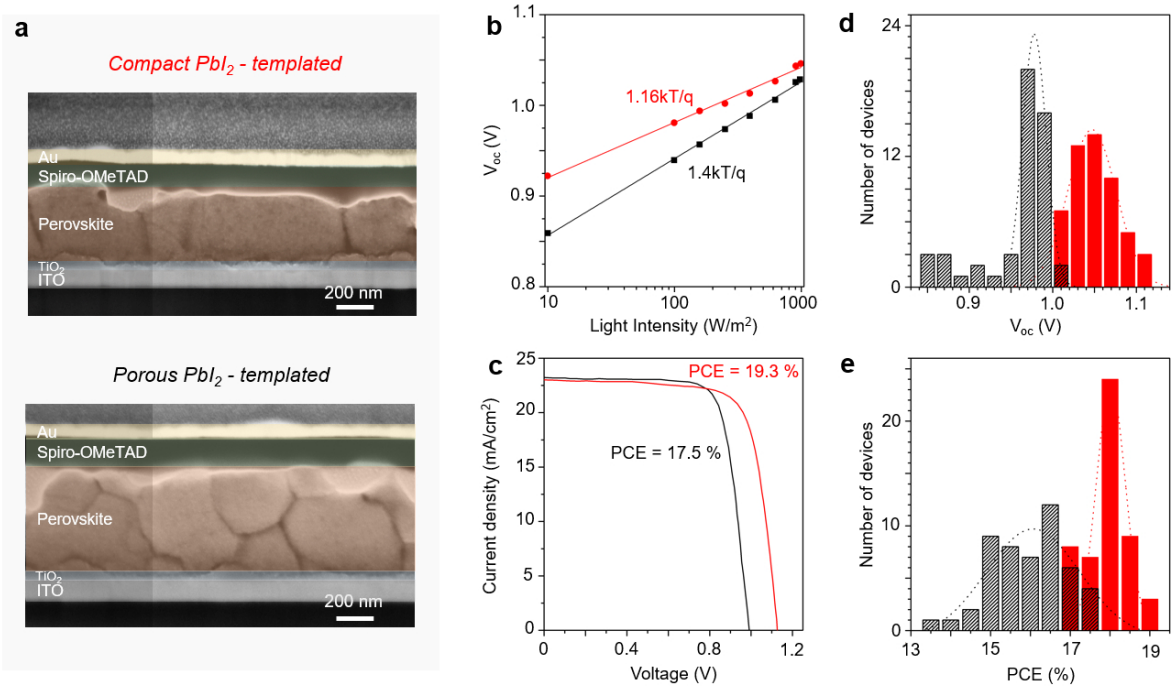

Figure 4. Structure and photovoltaic properties of solar cells based on perovskites fabricated with the compact PbI_2 – templated and porous – PbI_2 templated growth approaches. (a) Cross-section SEM images of selected solar cells produced by each approach. With the compact PbI_2 – templated growth approach, the perovskite consists of micro-crystals, with lateral dimensions beyond 1 µm. The crystal height is only limited by the layer thickness. With the porous PbI_2 – templated growth, the grains show smaller lateral dimensions (a few hundreds of nm). Furthermore, their height is smaller than the layer thickness. Instead, the layer consists of a stack of crystals separated by transverse grain boundaries. The white contrasts at the top interface of the perovskite layer stands for a thin and discontinuous PbI_2 self-passivation coating formed during the perovskite annealing. The absence of white contrast elsewhere in the perovskite layer supports the absence of unreacted PbI_2. This suggests that the PbI_2 signal in the XRD pattern of figure 1b originates only from the self-passivation at the top interface. Further data and explanations are given in Supporting Information S4 (Figure S4). (b) Light-intensity dependence of the V_{oc} of selected cells of both kinds, showing the relevant contribution of a trap-assisted recombination mechanism. This mechanism has a weaker impact for the compact PbI_2 – templated perovskite, yielding a higher V_{oc} at all light intensities. (c) J-V curves of the best cells of each kind, showing a higher V_{oc} and PCE for the compact PbI_2 – templated cell. (d) V_{oc} distribution and (e) PCE distribution measured for series of cells of the two types (compact PbI_2 – templated and porous PbI_2 – templated).

These images further evidence the dependence of the perovskite crystal size on the fabrication approach. In the compact PbI_2 - templated cell, the perovskite crystals are not only particularly large in the lateral directions (size superior to 1 μm), but also along the direction perpendicular to the substrate. Their height equals the thickness of the active perovskite layer, and the grain boundaries between crystals are vertical. In contrast, in the porous PbI_2 - templated cell, the active perovskite layer consists of a stack of crystals separated by transverse grain boundaries.

The larger perovskite crystals in the compact PbI_2 - templated cells and their lower non-radiative recombination probability correlate with a higher V_{oc}. This is illustrated in Figure 4b that shows the dependence of V_{oc} as a function of the incident photon flux below 1 sun, for a compact PbI_2 – templated cell and a porous PbI_2 – templated cell. A logarithmic relationship with a slope superior to kT/q is obtained for the cells fabricated following both approaches. This indicates the existence of a significant non-radiative trap-assisted recombination pathway. A smaller slope (1.16kT/q) is obtained for the compact PbI_2 - templated cell than for the porous PbI_2 - templated one (1.4kT/q) indicating less energy loss from non-radiative trap-assisted recombination in the former case. Such lower loss enables a higher V_{oc} at all photon fluxes in the investigated range.

While the perovskite fabrication approach impacts markedly the V_{oc} of the cells, it affects less their other photovoltaic parameters, in particular J_{sc}. This is examplified in Figure 4c that presents the optimal J-V curve of the best cell of each type. Both present similar J_{sc} values, which reflect a similar light harvesting performance that can be further analyzed from their EQE spectra (Supporting Information S5, Figure S5a). In contrast, a markedly higher V_{oc} is observed for the compact PbI_2 – templated cell (1.13 V vs 0.99 V). This higher V_{oc} is responsible for the higher PCE of this cell (19.3% vs 17.5%). Note that the higher performance of the compact PbI_2 – templated cell is also evidenced after stabilization in steady-state measurements, as shown in Supporting Information S5, Figure S5b, and that the compact PbI_2

– templated cell shows a better stability than the porous PbI_2 – templated one (Supporting Information S6, Figure S6).

The most probable values of V_{oc}, J_{sc}, FF and PCE obtained for the 50 cells of each type (Table 1) confirm that the examples above provide trends representative of the whole cell series. The V_{oc} of the compact PbI_2 – templated cell series is 8.3% higher than that of the porous PbI_2 – templated ones. In contrast, a smaller relative difference in J_{sc} and FF between the two cell series is found: it amounts to - 1.3% and 5.2%, respectively. Therefore, the 11.8% higher PCE observed for the compact PbI_2 – templated cell series results mainly from its higher V_{oc}. Such statistical correlation between V_{oc} and PCE is particularly clear from their distributions plotted in Figures 4d and 4e. Both distributions peak at smaller values for the porous PbI_2 – templated cell series (0.97 V, 16.1%) than for the compact PbI_2 – templated one (1.05 V, 18.0%), with a small overlap between both series.

Device type		**V_{oc} (V)**	**J_{SC} (mA/cm^2)**	**FF (%)**	**PCE (%)**
Compact PbI_2 - templated	*Best*	*1.13*	*23.0*	*74.6*	*19.3*
	50 devices	1.05±0.04	22.8±0.5	75.9±2.3	18.0±0.4
Porous PbI_2 - templated	*Best*	*0.99*	*23.2*	*76.2*	*17.5*
	50 devices	0.97±0.02	23.1±0.5	72.1±3.5	16.1±1.3

Table 1. Photovoltaic performance of the compact PbI_2 – templated and porous PbI_2 – templated solar cells. Best device and statistics over 50 devices (most probable value ± standard deviation).

3. DISCUSSION

Several recombination channels are responsible for the reduction in V_{oc}, which remains, even for the best perovskite solar cells,[1-5,11-16] significantly lower than the ideal one. Among these channels, the importance of non-radiative recombination[18,45,46] especially at interfaces,[18,45] has been underlined. Here, we may assume that the main difference seen in V_{oc} between the compact PbI_2 – templated and porous PbI_2 – templated cells of the current work has its origin

at the crystal interfaces within the bulk of the perovskite layer. For the larger crystals in the compact PbI_2 – templated cells the total interface area is reduced and consequently the number of surface charge trapping states is reduced, too. The rest of recombination channels should be similar for both types of cells, as similar compositions for the preparation of the active layer and the same charge transporting layers were used.

As shown in the Supporting Information S7, the interface trap recombination current density can be directly compared to the current densities linked to direct recombination either radiative or non-radiative. Then, given that the bandgap of both types of perovskites (and thus the ideal V_{oc}'s of the corresponding cells) are similar as discussed above, one may predict that the difference in V_{oc} between both cells should be proportional to the natural logarithm of the external fluorescence quantum yields ratio:

$$\Delta V_{oc} = V_{oc}^{compact} - V_{oc}^{porous} = \frac{kT}{q} Ln\left(\frac{f^{compact}}{f^{porous}}\right) \qquad (1)$$

where k is the Boltzmann constant, q the electrical charge, T the cell temperature, $V_{oc}^{compact}$ and V_{oc}^{porous} correspond to the open circuit voltages for the compact PbI_2 – templated and porous PbI_2 – templated cells, respectively, while $f^{compact}$ and f^{porous} are the external fluorescence quantum yields of the compact PbI_2 – templated and porous PbI_2 – templated cells, respectively. At 1 sun the external fluorescence quantum yield ratio is taken equal to 5, as extracted from Figure 3b. Then, using Equation (1) we may determine that the ΔV_{OC} would amount to 40 mV, which falls within one standard deviation of the difference between the most probable measured V_{oc} values (70 mV ± 50 mV), as can be seen in Figure 4d. One should note that, in general, there is a large dispersion in the reported V_{oc}'s from cells fabricated under the same exact conditions, and that higher V_{oc}'s than the one measured for the compact PbI_2 - templated cells have been reported in the past.[1-5] However, what is relevant is that the ΔV_{oc} we measured amounting to 70 mV corresponds to the difference in the most probable values for the open circuit voltages from two types of cells fabricated in similar conditions but, with a controllable

and well-defined difference in the size of the crystals. This is a confirmation that the compact PbI_2 – templated growth path we followed leads to a significant and clearly measureable increase in V_{oc} that can be directly linked to a measured increase in the external fluorescence quantum yield. Such increases are enabled by the larger crystal size that reduces the interface area and thus the density of interface non-radiative recombination pathways. Using Equation (1) again, it is estimated that the highest V_{oc} (1.13 V) achieved in this work lags only 80 mV below the ideal, radiative limit value that corresponds to a 100% external fluorescence quantum yield for the perovskite crystals. This highest achieved V_{oc} value is equivalent to 93% of the ideal one.

The trends found for FF and J_{sc} (Table 1) are consistent with theoretical expectations. Theoretical works that quantified the dependence on V_{oc}, FF and J_{sc} on trap density in perovskite solar cells indeed show that, at the relatively low trap densities of the perovskites we fabricated, a decrease in trap density induces a smaller relative increase in FF than in V_{oc}, and no sizeable effect on J_{sc}.[46, 47] Changing the trap density has a smaller effect on FF because, at the maximum power point, the photocarrier density in the perovskite is small so that traps are in excess. This excess remains upon decreasing the trap density, so that photocarrier concentration in the perovskite and thus the outgoing current experience a small increase only. Changing the trap density has no sizeable effect on J_{sc} because, at short-circuit, the internal electric field of the solar cell overcomes by far the coulombic field of the traps. Therefore, photocarriers do almost not interact with the traps, so that decreasing the trap density has no effect on charge extraction.

4. CONCLUSION

Summarizing, we have developed a solution-processing fabrication approach based on the two-step method to produce, in a well-controllable way, $FA_{0.8}MA_{0.2}PbI_3$ perovskite layers with high-quality crystals larger than 1 μm. By using a compact PbI_2 layer as template for the infiltration of the organic precursor, the limitations on the final perovskite crystal size intrinsic

to the standard porous PbI_2 - templated growth approach are overcome. We have shown that specific conditions, including the use of a highly concentrated organic precursor solution, Cl^- addition, and a post spin-coating solvent annealing must be combined to enable the efficient incorporation of the large FA^+ cation into the PbI_2 lattice, a full PbI_2 – to – perovskite conversion, and an efficient crystal growth. Note that such approach can also be applied to fabricate high quality perovskites with other compositions, for instance the triple cation ones.

Owing to the efficient incorporation of FA^+ ions, the fabricated crystals present a smaller band gap than the $MAPbI_3$ perovskite. They show no trace of any inactive wide band gap hexagonal phase. In relation with its larger crystal size than the porous PbI_2 – templated perovskite, the compact PbI_2 – templated perovskite shows a higher external fluorescence quantum yield (near 4% under 1 sun – equivalent illumination, and near 20% at saturation under 70 – sun equivalent illumination). Such more intense fluorescence reveals a higher contribution of radiative recombination, i.e. a lower non-radiative recombination probability.

Our results point at the importance of minimizing non-radiative recombination on defects at interfaces within the active layer of perovskite solar cells. This enables obtaining a high fluorescence quantum yield that correlates with a high V_{oc}. Such minimization can be achieved by reducing the total area of such interfaces by increasing the crystal size[44] as an alternative to or in combination with processes for the passivation of defects at interfaces.[18,48-50] Note that thanks to passivation, high fluorescence quantum yield and V_{oc} were demonstrated with relatively small crystals (sizes of a few hundreds of nm only).[50] Other ways to achieve increased fluorescence quantum yield and V_{oc} have been reported in the literature, such as using a perovskite with an in-depth heterogeneous composition.[51] A similar effect might occur when growing our mixed cation perovskite from a thicker porous PbI_2 – template.[52] However, the most natural and direct approach to reach the radiative limit, and ultimately the Shockley-Queisser optimum consists in growing large crystals with the suitable composition, followed by an interface passivation.

In this aspect, the compact PbI_2 – templated growth approach we have used is particularly relevant. It opens the way to increasing in a well controllable way the perovskite crystal size over 1 µm, together with incorporating large FA^+ cations. This enables at the same time bringing V_{oc} towards its radiative limit value, and decreasing the bandgap below that of the $MAPbI_3$ perovskites thus improving the absorption of near infrared photons and increasing J_{sc}. The achieved V_{oc} reaches 93% of the radiative value. This corresponds to a V_{oc} loss (voltage loss with respect to the electron charge times the bandgap of the perovskite, or $qE_g - V_{oc}$, see details in Supporting Information S8) of 0.40 V, which, as shown in Figure 5, is one of the lowest reported for hybrid lead halide perovskites.[13, 18, 53-55] Remarkably, such low V_{oc} loss is achieved with a perovskite with low bandgap of 1.53 eV. Therefore, the best device we fabricated is among the closest from the (E_g, $V_{oc,loss}$) Shockley-Queisser optimum. In this aspect, its performance is comparable with that of the best devices fabricated by two-step approaches.[53-55]

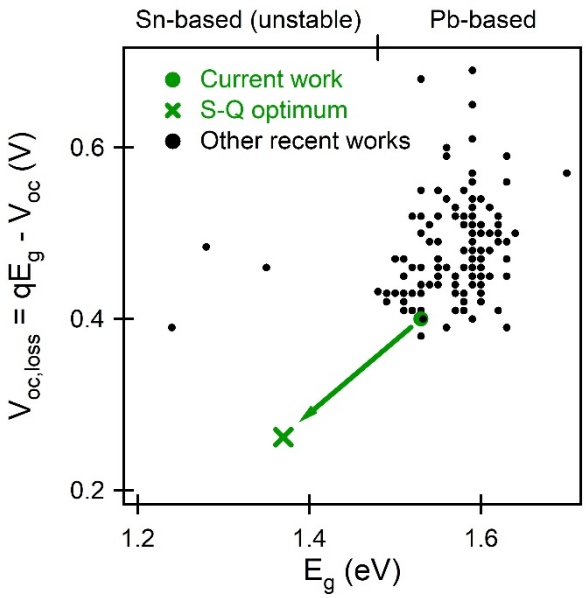

Figure 5. $V_{oc,loss}$ versus E_g for the best cell of the current work (green circle), compared with the values of cells found in the most recent state of the art literature (black dots). The Shockley-Queisser optimum (E_g = 1.35 eV and $V_{oc} = V_{oc,rad}$) is shown as a green cross.

METHODS

Solar cell fabrication. The commercial ITO glasses (15 Ω/sq) were cleaned in cleaning agent, deionized water, acetone, and isopropanol under sonication for 10 min in sequence, then treated by UV-ozone plasma for 10 min. The ETL of titanium diisopropoxide bis(acetylacetonate) (Sigma-Aldrich) stabilized TiO_2 nanoparticle solution (4-8 nm diameter, 20 wt% in water, PlasmaChem GmbH) was coated on ITO substrate at 6000 r.p.m. and annealed at 150 °C for 30 min in air. The thickness of the ETL is around 50 nm. The perovskite layer was then deposited by a sequential two-step spin coating method; first, 1.0 M of PbI_2 (99%, Sigma-Aldrich) in anhydrous N, N- Dimethylformamide (DMF) (99.8%, Sigma Aldrich) was spin coated onto the ETL at 2500 r.p.m. for 30 s. To prepare a compact PbI_2 film, the substrate was moved to a hotplate immediately after the spin-coating and annealed at 100 °C for 10 min to remove the remaining solvent; In contrast, to prepare a porous PbI_2 film, the as spun film was kept at a closed environment (covered by a petri dish) to retard the solvent evaporation for 10 min and then annealed at 100 °C for 10 min. Second, after the PbI_2 coated substrates cooling to room temperature (25 °C), 0.3 M of $CH(NH_2)_2I$ (98%, Sigma Aldrich) in 1 ml isopropanol with 10 mol % of CH_3NH_3Cl (Sigma Aldrich) was spin coated onto the PbI_2 at 2500 r.p.m. for 45 s, and then annealed at 150 °C for 20 min without (thermal annealing) or with (solvent annealing) the presence of small amount (5 μL) DMF in a closed environmental. The HTL solution was prepared by dissolving 72.3 mg (2,2',7,7'-tetrakis-(N,N-dimethoxyphenylamine)-9,9'-spirobifluorene) (Spiro-OMeTAD, Merck), 28.9 mL 4-tert-butylpyridine (99.9%, Sigma-Aldrich) and 17.5 mL of a stock solution of 520 mg/ml lithium bis(trifluoromethylsulphonyl)imide in acetonitrile (99.9%, Sigma-Aldrich) in 1 mL chlorobenzene (99.9%, Sigma-Aldrich). The ~200 nm thick HTL was deposited by spin coating the solution at 3000 r.p.m. for 45 s, and the solution concentration and spin coating speed were varied to achieve thinner thickness. Finally, the Au (80 nm, 1 $Å \cdot s^{-1}$) was deposited by thermal

evaporation under a pressure of $<5\times10^{-6}$ mBar. The active area was 0.096 cm^2 measured by optical microscopy.

Structural characterization. The XRD patterns of the perovskite films were characterized with a Bruker D8 diffractometer in the Bragg-Brentano (θ-2θ) configuration. The top-view SEM images of the perovskite films were obtained by field emission scanning electron microscopy (FEG-SEM, FEI Inspect F-EBL). For the cross-sectional observation of the device structure, a Zeiss Auriga setup was used. It combines a Ga focused ion beam (FIB) for cross-section preparation and scanning electron microscopy (SEM) functionalities for specimen observation. A layer of Pt was firstly deposited on the surface to protect the top structure from FIB milling. Then the materials were subsequently milled by Ga FIB at 30 kV, with currents of 1 nA for coarse milling and 50 pA for fine milling. The cross section was then observed by SEM at 54º with acceleration voltage of 5 kV and an aperture of 30 μm.

Fluorescence spectra and fluorescence quantum yield. The sample was placed inside a 4-port integrating sphere, with the perovskite layer being in contact with the Spectralon sample holder located at the port facing the input one. The incident light emitted by a continuous wave (cw) Nd:YAG laser (532 nm), incoming from the input port, was therefore impinging onto the sample from the side of the glass substrate so that it pumped the perovskite layer after crossing the glass and TiO_2 layer. The sample was tilted of a few degrees from the incident beam to ensure that the light reflected by it could not escape directly through the input port. A fibered spectrometer connected to the 3rd port of the integrated sphere was used to record the perovskite fluorescence spectrum. A calibrated Si detector connected to the 4th port of the integrating sphere was used to perform the external fluorescence quantum yield measurements. To achieve such measurements, suitable optical filters were placed alternatively between the port of the integrating sphere and the detector to separate the contributions of the scattered/reflected light (λ_{scatt} = 532 nm) and of the perovskite fluorescence (λ_{fluo} # 810 nm). After correcting for the

filter transmittance, one obtains the scattered power P_{scatt} and the fluorescence power P_{fluo} for the measured sample. After measuring the reference signals $P_{scatt, ref}$ and $P_{fluo, ref}$ (Spectralon sample holder without sample), the external fluorescence quantum yield f (in %) was obtained from the relation:

$$f = 100 \frac{\lambda_{fluo}}{\lambda_{scatt}} \left(\frac{P_{fluo} - P_{fluo,ref}}{P_{scatt,ref} - P_{scatt}} \right) \qquad (2)$$

The fluorescence quantum yield was measured for different values of incident photon flux, controlled by using combinations of optical density filters mounted on filter wheels placed along the optical path. The measurements were done with a gradually increasing photon flux, and the beam was blocked by a shutter between each measurement. At the lowest photon fluxes (a few sun – equivalent), an increasing transient of the fluorescence signal was observed on the time scale of seconds. The power values were recorded after stabilization. At the highest photon fluxes (several tens of sun-equivalent), no increasing transient was observed but a decrease in the fluorescence signal was observed after near 10 s. In this case, the power values were recorded immediately after opening the shutter. Note that, to ensure that steady state conditions could be reached, the measurements were done in purely continuous conditions, i.e. without any modulation nor lock-in amplification of the incident cw light.

Photovoltaic characterization of the solar cells. The current density-voltage (J-V) characteristics were measured using a Keithley 2400 SourceMeter under the illumination of the solar simulator (ABET Sol3A) at the light intensity of 100 $mW \cdot cm^{-2}$ which was adjusted with a monocrystalline silicon reference cell (Hamamatsu) calibrated at the Fraunhofer Institute for Solar Energy Systems. The measurements were carried out in the ambient atmosphere with a scanning rate of 10 $mV \cdot s^{-1}$. Both scanning directions (forward and reverse) were measured to check the hysteresis effect of the device. The steady-state measurements were performed by setting the bias voltage to the voltage at maximum power point (V_{MPP}, determined from the J-V curves) and then tracing the current density as function of time during 60 seconds. The device

stability was studied by monitoring the J-V characteristics of the cells under 1 sun light illumination, the illumination was carried out in the glovebox and the J-V measurement was performed in air condition. EQE values were measured using a quantum efficiency measurement system (QEX10, PV Measurements). The spectral response of the calibrated silicon cell was used as a reference. Transient photovoltage (TPV) of the devices were measured with an in-house-built set-up. The set-up comprises a LED lamp to provide steady state white bias light, a 637 nm wavelength laser (Vortran Stradus) and an Agilent 4000X oscilloscope. The LED lamp was used to get steady V_{OC} of the device. The intensity of the laser was controlled to keep the voltage transient amplitude under 5% of the steady state light bias. The oscilloscope records the data using 1 MΩ input impedance for the TPV measurement.

ASSOCIATED CONTENT

Supporting Information

The Supporting Information is available free of charge on the ACS Publications website at DOI: 10.1021/xxxx. S1. Process flow and perovskite formation mechanism with the compact PbI_2 – templated and porous PbI_2 – templated growth approaches. S2. Fabrication, structure and optical properties of the compact PbI_2 – templated $FA_{0.8}MA_{0.2}PbI_3$ perovskite layer. S3. Comparison of the structure and optical properties of the compact PbI_2 – templated and porous PbI_2 – templated $FA_{0.8}MA_{0.8}PbI_3$ perovskite layers. S4. Supplementary cross-section SEM images of the "compact PbI_2 – templated perovskite solar cell. S5. Complementary photovoltaic characterization of the compact PbI_2 – templated and porous PbI_2 – templated perovskite solar cells. S6. Stability of the compact PbI_2 – templated and porous PbI_2 – templated perovskite solar cells. S7. Relation between V_{oc} and fluorescence quantum yield in perovskite solar cells with surface trapping states. S8. V_{oc} loss of solar cells.

AUTHOR INFORMATION

Corresponding Author

*E-mail: iamhuizhang@njtech.edu.cn

*E-mail: johann.toudert@icfo.eu

*E-mail: jordi.martorell@icfo.eu

Author Contributions

H.Z. prepared the perovskite films and solar cells and performed the basic and photovoltaic characterization. G. M.-D. did the top-view SEM characterization. J.O. did the cross-section SEM characterization. M.K. and J.T. designed the fluorescence quantum yield experiments

and performed the measurements. J.M. did the fluorescence quantum yield modelling and coordinated the work. All the authors discussed the results and commented on the manuscript.

ACKNOWLEDGMENTS

The authors (H.Z., M.K., G.M.-D., J.O., J.T. & J.M.) acknowledge financial support from the Spanish Ministry of Economy and Competitiveness through the "Severo Ochoa" program for Centres of Excellence in R&D (SEV-2015-0522), from Fundació Privada Cellex, and from Generalitat de Catalunya through the CERCA program. The authors (H.Z., M.K., G.M.-D., J.O., J.T. & J.M.) acknowledge financial support from the Spanish Ministry of Economy and Competitiveness (MAT2017-89522-R). H.Z. acknowledges financial support from the Chinese Natural Science Foundation of Jiangsu Province (BK20171022) and the Scientific Research Foundation for the Returned Overseas Chinese Scholars.

REFERENCES

(1) Green, M.A.; Hishikawa, Y.; Dunlop, E.D.; Levi, D.H.; Hohl-Ebinger, J.; Yoshita, M.; Ho-Baillie, A.W.Y. Solar Cell Efficiency Tables (version 53) *Prog. Photovolt. Res. Appl.* **2018**, *27*, 3-12.

(2) Bi, D.; Yi, C.; Luo, J.; Décoppet, J.D.; Zhang, F.; Zakeeruddin, S.; Li, X.; Hagfeldt, A.; Grätzel, M. Polymer-templated Nucleation and Crystal Growth of Perovskite Films for Solar Cells with Efficiency Greater than 21% *Nat. Energy* **2016**, *1*, 16142.

(3) Zheng, X.; Chen, B.; Dai, J.; Fang, Y.; Bai, Y.; Lin, Y.; Wei, H.; Zeng, X.C.; Huang, J. Defect Passivation in Hybrid Perovskite Solar Cells Using Quaternary Ammonium Halide Anions and Cations *Nat. Energy* **2017**, *2*, 17102.

(4) Tan, H.R.; Jain, A.; Voznyy, O.; Lan, X.; Pelayo Garcia de Arquer, F.; Fan, J.Z.; Quintero-Bermudez, R.; Yuan, M.; Zhang, B.; Zhao, Y.; Fan, F.; Li, P.; Quan, L.N.; Zhao, Y.; Lu, Z.-H.; Yang, Z.; Hoogland, S.; Sargent, E.H. Efficient and Stable Solution-processed Planar Perovskite Solar Cells via Contact Passivation *Science* **2017**, *355*, 722-726.

(5) Correa-Baena, J.P.; Saliba, M.; Buonassisi, T.; Grätzel, M.; Abate, A.; Tress, W.; Hagfeldt, A. Promises and Challenges of Perovskite Solar Cells *Science* **2017**, *358*, 739-744.

(6) Green, M.A.; Hishikawa, Y.; Dunlop, E.D.; Levi, D.H.; Hohl-Ebinger, J.; Ho-Baillie, A.W.Y. Solar Cells Efficiency Tables (version 51) *Prog. Photovolt. Res. Appl.* **2018**, *26*, 3-12.

(7) Shockley, W.; Queisser, H.J. Detailed Balance Limit of Efficiency of p-n Junction Solar Cells *J. Appl. Phys.* **1961**, *32*, 510.

(8) Eperon, G.E.; Stranks, S.D.; Menelaou, C.; Johnston, M.B.; Herz, L.M.; Snaith, H.J. Formamidinium Lead Trihalide: a Broadly Tunable Perovskite for Efficient Planar Heterojunction Solar Cells *Energy Environ. Sci.* **2014**, *7*, 982-988.

(9) Yang, W.S.; Noh, J.H.; Jeon, N.J.; Kim, Y.C.; Ryu, S.; Seo, J.; Seok, S.I. High-Performance Photovoltaic Perovskite Layers Fabricated through Intramolecular Exchange *Science* **2015**, *348*, 1234-1237.

(10) Binek, A.; Hanusch, F.C.; Docampo, P.; Bein, T. Stabilization of the Trigonal High-temperature Phase of Formamidinium Lead Iodide *J. Phys. Chem. Lett.* **2015**, *6*, 1249-1253.

(11) Bi, D.; Tress, W.; Dar, M.I.; Gao, P.; Luo, J.; Renevier, C.; Schenk, K.; Abate, A.; Giordano, F.; Correa Baena, J.-P.; Decoppet, J.-D.; Zakeeruddin, S.M.; Nazeeruddin, M.K.; Grätzel, M.; Hagfeldt, A. Efficient Luminescent Solar Cells Based on Tailored Mixed-Cation Perovskites *Sci. Adv.* **2016**, *2*, e1501170.

(12) Jacobsson, T.J.; Correa-Baena, J.-P.; Pazoki, M.; Saliba, M.; Schenk, K.; Grätzel, M.; Hagfeldt, A. Exploration of the Compositional Space for Mixed Lead Halogen Perovskites for High Efficiency Solar Cells *Energy Environ. Sci.* **2016**, *9*, 1706-1724.

(13) Saliba, M.; Matsui, T.; Domanski, K.; Seo, J.-Y.; Ummadisingu, A.; Zakeeruddin, S.M.; Correa-Baena, J.P.; Tress, W.R.; Abate, A.; Hagfeldt, A.; Grätzel, M. Incorporation of Rubidium Cations into Perovskite Solar Cells Improves the Photovoltaic Performance *Science* **2016**, *354*, 206-209

(14) Conings, B.; Babayigit, A.; Klug, M.T.; Bai, S.; Gauquelin, N.; Sakai, N.; Wang, J.T.-W.; Verbeeck, J.; Boyen, H.G.; Snaith, H. A. Universal Deposition Protocol for Planar Heterojunction Solar Cells with High Efficiency Based on Hybrid Lead Halide Perovskite Families *Adv. Mater.* **2016**, *28,* 10701-10709.

(15) Zhang, M.; Yun, J.S.; Ma, Q.; Zheng, K.; Lau, C.F.J.; Deng, X.; Kim, J.; Kim, D.; Seidel, J.; Green, M.A.; Huang, S.; Ho-Baillie, A.W.Y. High-efficiency Rubidium-incorporated Perovskite Solar Cells by Gas Quenching *ACS Energy Lett.* **2017**, *2*, 438-444.

(16) Weber, O.J.; Charles, B.; Weller, M.T. Phase Behaviour and Composition in the Formamidinium-methylammonium Hybrid Lead Iodide Perovskite Solid Solution *J. Mater. Chem.* **2016**, *4*, 15375-15382.

(17) Ha, S.-T.; Chen, C.; Zhang, J.; Xiong, Q. Laser Cooling of Organic-inorganic Lead Halide Perovskites *Nat. Photon.* **2016**, *10*, 115-121.

(18) Abdi-Jalebi, M.; Andaji-Garmaroudi, Z.; Cacovich, S.; Stravakas, C.; Philippe, B.; Richter, J.M.; Alsari, M.; Booker, E.P.; Hutter, E.M.; Pearson, A.J.; Lilliu, S.; Savenije, T.J.; Rensmo, H.; Divititi, G.; Ducati, C.; Friend, R.H.; Stranks, S.D. Maximizing and Stabilizing Luminescence from Halide Perovskites with Potassium Passivation *Nature* **2018**, *555*, 497-501.

(19) Yang, Y.; Yan, Y.; Yang, M.; Choi, S.; Zhu, K.; Luther, J.M.; Beard, M.C. Low Surface Recombination Velocity in Solution-grown $CH_3NH_3PbBr_3$ Perovskite Single Crystal *Nat. Commun.* **2015**, 7961.

(20) Burschka, J.; Pellet, N.; Moon, S.-J.; Humphry-Baker, R.; Gao, P.; Nazeeruddin, M.K.; Gratzel, M. Sequential Deposition as a Route to High-performance Perovskite-sensitized Solar Cells *Nature* **2013**, *499*, 316-319.

(21) Chen, H. Two-step Sequential Deposition of Organometal Halide Perovskite for Photovoltaic Application *Adv. Funct. Mater.* **2017**, *27*, 1605654.

(22) Liu, T.; Hu, Q.; Wu, J.; Chen, K.; Zhao, L.; Liu, F.; Wang, C.; Lu, H.S.; Jia, S.; Russell, T.R.; Zhu, R.; Gong, Q. Mesoporous PbI_2 Scaffold for High-performance Planar Heterojunction Perovskite Solar Cells *Adv. Energy Mater.* **2016**, *6*, 1501890.

(23) Xiao, Z.; Dong, Q.; Bi, C.; Shao, Y.; Yuan, Y.; Huang, J. Solvent Annealing of Perovskite-induced Crystal Growth for Photovoltaic-device Efficiency Enhancement *Adv. Mater.* **2014**, *26*, 6503-6509.

(24) Zheng, H.; Wang, W.; Yang, S.; Liu, Y.; Sun, J. A Facile Way to Prepare Nanoporous PbI_2 Films and their Application in Fast Conversion to $CH_3NH_3PbI_3$ *RSC Adv.* **2016**, *6*, 1611-1617.

(25) Xiong, H.; DeLuca, G.; Rui, Y.; Li, Y.; Reichmanis, E.; Zhang, Q.; Wang, H. Solvent Vapor Annealing of Oriented PbI_2 Films for Improved Crystallization of Perovskite Films in the Air *Sol. Energy. Sol. Cells* **2017**, *166*, 167-175.

(26) Ono, L.K.; Juarez-Perez, E.J.; Qi, Y. Progress on Perovskite Materials and Solar Cells with Mixed Cations and Halide Anions *ACS Appl. Mater. Interfaces* **2017**, *9*, 30197-30246.

(27) Li, L.; Liu, N.; Xu, Z.; Chen, Q.; Wang, X.; Zhou, H. Precise Composition Tailoring of Mixed-cation Hybrid Perovskites for Efficient Solar Cells by Mixture Design Methods *ACS Nano* **2017**, *11*, 8804-8813.

(28) Yang, W.S.; Noh, J.H.; Jeon, N.J.; Kim, Y.C.; Ryu, S.; Seo, J.; Seok, S.I. High-performance Photovoltaic Perovskite Layers Fabricated Through Intramolecular Exchange *Science* **2015**, *348*, 1234-1237.

(29) Zheng, X.; Wu, C.; Jha, S.K.; Li, Z.; Zhu, K.; Priya, S. Improved Phase Stability of Formamidinium Lead Triiodide Perovskite by Strain Relaxation *ACS Energy Lett.* **2016**, *1*, 1014-1020.

(30) Pellet, N.; Gao, P.; Gregori, G.; Yang, T.-Y.; Nazeeruddin, M.K.; Maier, J.; Grätzel, M. Mixed-organic-cation Perovskite Photovoltaics For Enhanced Solar-light Harvesting *Angew. Chem. Int. Ed.* **2014**, *53*, 3151-3157.

(31) Li, C.; Guo, Q.; Zhang, H.; Bai, Y.; Wang, F.; Liu, L.; Hayat, T.; Alsaedi, A.; Tan, Z. Enhancing the Crystallinity of $HC(NH_2)_2PbI_3$ Film by Incorporating Methylammonium Halide Intermediate for Efficient and Stable Perovskite Solar Cells *Nano Energy* **2017**, *40*, 248-257.

(32) Zhou, N.; Shen, Y.; Zhang, Y.; Xu, Z.; Zheng, G.; Li, L.; Chen, Q.; Zhou, H. CsI Pre-intercalation in the Inorganic Framework for Efficient and Stable $FA_{1-x}Cs_xPbI_3(Cl)$ Perovskite Solar Cells *Small* **2017**, *13*, 1700484.

(33) Dong, Q.; Yuan, Y.; Shao, Y.; Fang, Y.; Wang, Q.; Huang, J. Abnormal Crystal Growth in $CH_3NH_3PbI_{3-x}Cl_x$ using a Multi-cycle Solution Coating Process *Energy. Environ. Sci.* **2015**, *8*, 2464-2470.

(34) Wu, C.-G.; Chiang, C.-H.; Tseng, Z.-L.; Nazeeruddin, M.K.; Hagfeldt, A.; Grätzel, M. High Efficiency Stable Inverted Perovskite Solar Cells without Current Hysteresis *Energy Environ. Sci.* **2015**, *8*, 2725-2733.

(35) Fu, Y.; Meng, F.; Rowley, M.B.; Thompson, B.J.; Shearer, M.J.; Ma, D.; Hamers, R.J.; Wright, J.C.; Jin, S.J. Solution Growth of Single Crystal Methylammonium Lead Halide Perovskite Nanostructures for Optoelectronic and Photovoltaic Applications *J. Am. Chem. Soc.* **2015**, *137*, 5810-5818.

(36) Xu, Y.; Zhu, L.; Shi, J.; Lv, S.; Xu, X.; Xiao, J.; Dong, J.; Luo, Y.; Li, D.; Meng, Q. Efficient Hybrid Mesoscopic Solar Cells with Morphology-controlled $CH_3NH_3PbI_{3-x}Cl_x$ Derived from Two-step Spin Coating Method *ACS Appl. Mater. Interfaces* **2015**, *7*, 2242-2248.

(37) Dong, Q.; Yuan, Y.; Shao, Y.; Fang, Y.; Wang, Q.; Huang, J. Abnormal Crystal Growth in $CH_3NH_3PbI_{3-x}Cl_x$ using a Multi-cycle Solution Coating Process *Energy Environ. Sci.* **2015**, *8*, 2464-2470.

(38) Jiang, F.; Rong, Y.; Liu, H.; Liu, T.; Mao, L.; Meng, W.; Qin, F.; Jiang, Y.; Luo, B.; Xiong, S.; Tong, J.; Liu, Y.; Li, Z.; Han, H.; Zhou, Y. Synergistic Effect of PbI_2 Passivation and Chlorine Inclusion Yielding Open-circuit Voltage Exceeding 1.15V in both Mesoscopic and Inverted Planar $CH_3NH_3PbI_3$(Cl)-based Perovskite Solar Cells *Adv. Funct. Mater.* **2016**, *26*, 8119-8127.

(39) Xiao, Z.; Dong, Q.; Bi, C.; Shao, Y.; Yuan, Y.; Huang, J. Solvent Annealing of Perovskite-induced Crystal Growth for Photovoltaic-device Efficiency Enhancement *Adv. Mater.* **2014**, *26*, 6503-6509.

(40) Liu, C.; Wang, K.; Yi, C.; Shi, X.; Smith, A.W.; Gong, S.; Heeger. A.J. Efficient Perovskite Hybrid Photovoltaics via Alcohol-vapor Annealing Treatment *Adv. Funct. Mater.* **2016**, *26*, 101-110.

(41) Tress, W. Perovskite Solar Cells on the Way to their Radiative Efficiency Limit – Insights into a Success Story of High Open-circuit Voltage and Low Recombination *Adv. Energy Mater.* **2017**, *7*, 1602358.

(42) Sutter-Fella, C.M.; Li, Y.; Amani, M.; Ager III, J.W.; Toma, F.M.; Yablonovitch, E.; Sharp, I.D.; Javey, A. High Photoluminescence Quantum Yield in Band Gap Tunable Bromide Containing Mixed Halide Perovskites *Nano Lett.* **2016**, *16*, 800-806.

(43) Richter, J.A.; Abdi-Jalebi, M.; Sadhanala, A.; Tabachnyk, M.; Rivett, J.P.H.; Pazos-Outón, L.M.; Gödel, K.C.; Dechsler, F.; Friend, R. Enhancing Photoluminescence Yields in Lead Halide Perovskites by Photon Recycling and Light Out-coupling *Nat. Commun.* **2016**, *7*, 13941.

(44) Stranks, S.D.; Burlakov, V.M.; Leitjens, T.; Ball, J.M.; Goriely, A.; Snaith, H. Recombination Kinetics in Organic-inorganic Perovskites: Excitons, Free Charges, and Subgap States *Phys. Rev. Appl.* **2014**, *2*, 034007.

(45) Sherkar, T.S.; Momblona, C.; Gil-Escrig, L.; Avila, J.; Sessolo, M.; Bolink, H.J.; Anton Koster, L.J. Recombination in Perovskite Solar Cells: Significance of Grain Boundaries, Interface Traps, and Defect Ions *ACS Energy Lett.* **2017**, *2*, 1214 – 1222.

(46) Pazos-Outón, L.M.; Xiao, T.P.; Yablonovitch, E. Fundamental Efficiency Limits of Lead Halide Perovskite Solar Cells *J. Phys. Chem. Lett.* **2018**, *9*, 1703-1711.

(47) Minemoto, T.; Murata, M. Device Modelling of Perovskite Solar Cells Based on Structural Similarity with Thin Film Inorganic Semiconductor Solar Cells *J. Appl. Phys.*, **2014**, *116*, 054505.

(48) Noel, N.K.; Abate, A; Stranks, S.D.; Parrott, E.S.; Burlakov, V.M.; Goriely, A.; Snaith, H.J. Enhanced Photoluminescence and Solar Cell Performance via Lewis Base Passivation of Organic-inorganic Lead Halide Perovskites *ACS Nano*, **2014**, *8*, 9815-9821.

(49) deQuilettes, D.W.; Koch, S.; Burke, S.; Paranji, R.K.; Shropshire, A.J.; Ziffer, M.E.; Ginger, D.S. Photoluminescence Lifetimes Exceeding 8 μs and Quantum Yields Exceeding 30% in Hybrid Perovskite Thin Films by Ligand Passivation *ACS Energy Lett.* **2016**, *1*, 438-444.

(50) Braly, I.L.; deQuilettes, D.W.; Pazos-Outón, L.M.; Burke, S.; Ziffer, M.E.; Ginger, D.S.; Hillhouse, H.W. Hybrid Perovskite Films Approaching the Radiative Limit with Over 90% Photoluminescence Quantum Efficiency *Nat. Photon.* **2018**, *12*, 355-361.

(51) Luo, D.; Yang, W.; Wang, Z.; Sadhanala, A.; Hu, Q.; Su, R.; Shivanna, R.; Trindade, G.F.; Watts, J.F.; Xu, Z.; Liu, T.; Chen, K.; Ye, F.; Wu, P.; Zhao, L.; Wu, J.; tu, Y.; Zhang, Y.; Yang, X.; Zhang, W.; Friend, R.H.; Gong, Q.; Snaith, H.J.; Zhu, R. Enhanced Photovoltage for Inverted Planar Heterojunction Perovskite Solar Cells *Science* **2018**, *360*, 1442-1446.

(52) Zhang, H.; Kramarenko, M.; Osmond, J.; Toudert, J.; Martorell, J.; Natural Random Nanotexturing of the Au interface for Light Backscattering Enhanced Performance in Perovskite Solar Cells *ACS Photon.* **2018**, *5*, 2243-2245.

(53) Jiang, Q.; Chu, Z.; Wang, P.; Yang, X.; Liu, H.; Wang, Y.; Yin, Z.; Wu, J.; Zhang, X.; You, J. Planar-structure Perovskite Solar Cells with Efficiency Beyond 21% *Adv. Mater.* **2017**, *29*, 1703852.

(54) Zhao, Y.; Tan, H; Yuan, H.; Yang, Z.; Fan, J.Z.; Kim, J.; Voznyy, O.; Gong,X.; Quan, L.N.; Tan, C.S.; Hofkens, J.; Yu, D.; Zhao, Q.; Sargent, E.H. Perovskite Seeding Growth of formamidinium-lead-iodide-based perovskites for efficient and stable solar cells *Nature Commun.* **2018**, *9*, 1607.

(55) Zhao, Y.; Li, Q.; Zhou, W.; Hou, Y.; Zhao, Y.; Fu, R.; Yu, D.; Liu, X.; Zhao, Q. Double-side-passivated Perovskite Solar Cells with Ultra-low Potential Loss *Sol. RRL* **2018**, 1500296.

For Table of Contents